

Topological Quantum Computing Using Nanowire Devices

C. Tutschku¹, R. W. Reinthaler¹, C. Lei^{2,3}, A. H. MacDonald³, and E. M. Hankiewicz¹

¹*Faculty of Physics and Astrophysics and Würzburg-Dresden Cluster of Excellence ct.qmat, University of Würzburg, Germany*

²*Department of Modern Physics, University of Science and Technology of China, Hefei, China* and

³*Department of Physics, University of Texas at Austin, USA*

The boundary of topological superconductors might lead to the appearance of Majorana edge modes, whose non-trivial exchange statistics can be used for topological quantum computing. In branched nanowire networks one can exchange Majorana states by time-dependently tuning topologically non-trivial parameter regions. In this work, we simulate the exchange of four Majorana modes in T-shaped junctions made out of p-wave superconducting Rashba wires. We derive concrete experimental predictions for (quasi-)adiabatic braiding times and determine geometric conditions for successful Majorana exchange processes. Contrary to the widespread opinion, we show for the first time that in the adiabatic limit the gating time needs to be smaller than the inverse of the squared superconducting order parameter and scales linearly with the gating potential. Further, we show how to circumvent the formation of additional Majorana modes in branched nanowire systems, arising at wire intersection points of narrow junctions. Finally, we propose a multi qubit setup, which allows for universal and in particular topologically protected quantum computing.

I. INTRODUCTION

Topological quantum computing (TQC) represents a fault tolerant quantum computation scheme in which unitary quantum gates are realized by the braiding of so-called anyons, satisfying non-abelian exchange statistics¹. These operations are only dependent on the topological class of the braiding group element, leading to TQC algorithms, protected by the energy gap of the system. Such quantum gates remain robust to disturbance and local noise if braiding procedures are (quasi-)adiabatic and if external perturbations do not close this gap².

A special representative of non-abelian anyons are Majorana fermions (MFs), showing up as quasi-particle excitations in condensed matter physics¹. Exemplary, such states are predicted in $\nu = 5/2$ fractional quantum Hall states or in topologically non-trivial systems proximity-coupled to bulk superconductors, e.g. at the edge of 2D topological insulators (TIs), in nanowires made from 3D TIs, in magnetized helical spin chains, or in semi-conducting Rashba nanowires^{3–19}. Since 2012, Majorana modes in Rashba wires are of particular interest, caused by their experimental evidence in InSb nanowires²⁰. Up to this date, several other experiments showed an indication of Majorana fermions in solid state systems^{21–37}. In contrast to recent approaches of (teleportation or measurement based) Majorana braiding procedures on parallel or hexagonal nanowire structures^{38–48}, we simulate in this work spatial Majorana braiding procedures in p-wave superconducting nanowires, arranged as triple T-junctions^{49–52}. While we consider isolated geometries at zero temperature, the analysis of coupling those systems to parity-conserving thermal baths can be found in Refs. 53, 54. In particular, we derive geometric and adiabatic requirements for successfully exchanging multiple Majorana modes in branched nanowire devices. We analytically and numerically evaluate the functional dependence of the adiabatic exchange time on the superconducting order parameter as well as on the gating poten-

tial. Moreover, we propose a full nanowire-based setup which is suitable for universal quantum computing. Further, we analytically and numerically solve the problem of additional MF modes, forming at wire intersection points in branched nanowire based devices^{55,56}. In general, the formation of such modes prevents any successful topological qubit operation. We solve this serious problem by locally gating the wire intersection points.

This work is structured as follows: In Sec. II, we introduce the Bogoliubov-de Gennes (BdG) Hamiltonian, characterizing our exchange geometry. Moreover, we present various, different Majorana exchange protocols, defining TQC algorithms. In Sec. III, we discuss the exchange statistics of four MF modes, specifying a topological single qubit. In Sec. IV, we show that for narrow nanowire junctions, additional MF modes form at wire intersection points, and rigorously prove how to solve this effect. In Sec. V, we determine adiabatic time scales and geometric conditions for successful MF exchange protocols, enabling different single qubit operations. Moreover, we compare these results to existent adiabatic limits on MF exchange processes^{57–66}. In Sec. VI, we discuss the concept of universal TQC, introduce projective measurements and propose a nanowire setup, defining a Majorana based multi qubit system. Finally, we summarize our paper in Sec. VII.

II. MODEL & SETUP

Majorana edge modes are predicted at the boundaries of topological superconductors and are associated to local densities which exponentially decay into the bulk of the system^{50,67}. In general, these modes hybridize and form highly nonlocal Dirac fermionic states (HMFs). If γ_1 and γ_2 represent second quantized MF operators, the corresponding HMF modes are given by $\psi^{(\dagger)} = (\gamma_1 \pm i\gamma_2)/2$. Their energy Δ_{hyb} decreases exponentially with the spatial separation of $\gamma_{1,2}$. Experimentally, it is possible to engineer an effective p-wave superconductor by using

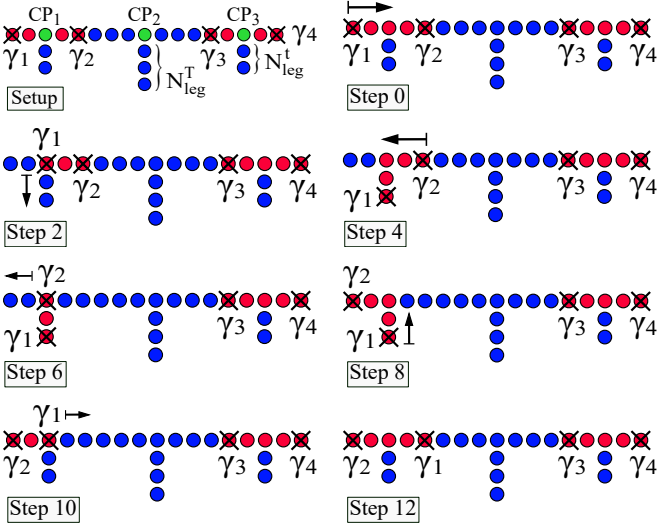


FIG. 1: Setup: Structure of a tTt device, consisting of 4 nanowires. The chemical potential on each site can be controlled by a "keyboard" gate. Inner and outer T/t structures are characterized by the amount of lattice sites N_{leg}^T and N_{leg}^t . Moreover, $\text{CP}_{1,2,3}$ denote nanowire intersection points and red (blue) regions encode topologically non-trivial (trivial) junction parts with associated MF modes $\gamma_{1,2,3,4}$. **Step 0-12** characterizes the exchange protocol $\gamma_1 \leftrightarrow \gamma_2$. With $N_{\text{leg}}^t = 2$, $N_{\text{leg}}^T = 3$ and $N_{\text{gate}} = 1$ the exchange is realized in 12 steps, corresponding to the different keyboard gate configurations.

a quasi one-dimensional nanowire with strong spin-orbit (SO) interaction. The additional ingredients for such a construction are a magnetic field, aligned along the axis of the nanowire and perpendicular to the SO field, and a proximitized s -wave superconductor^{20,67}. In the basis $[c_{\uparrow}^{\dagger}(k), c_{\downarrow}^{\dagger}(k), c_{\downarrow}(-k), -c_{\uparrow}(-k)]$, T-junctions based on nanowires are described by the BdG Hamiltonian:

$$H_{\text{BdG}} = \left[\left(\frac{\hbar^2}{2m_{\text{eff}}} (k_x^2 + k_y^2) - \mu \right) \tau_3 + \Delta_{\text{sc}} \tau_1 \right] \otimes \sigma_0 \quad (1) \\ + h_Z \tau_0 \otimes \sigma_3 + \alpha \tau_3 \otimes [k_x \sigma_2 + k_y \sigma_1].$$

Here, $\tau_{0,1,2,3}$ are Pauli matrices acting on the electron-hole subspace, while $\sigma_{0,1,2,3}$ are Pauli matrices, acting on spin degrees of freedom. $\Delta_{\text{sc}} = |\Delta_{\text{sc}}|e^{i\phi}$ is the s -wave order parameter and we choose $\phi = 0$ ($\phi = \pi/2$) for the superconducting phase in horizontal (\vec{e}_x (vertical \vec{e}_y) direction. Furthermore, μ is the chemical potential, $h_Z = g\mu_B B/2$ the Zeeman energy, g the Landé g -factor, μ_B the Bohr magneton, α the Rashba parameter and m_{eff} the effective electron mass in the nanowire. If one guarantees $|\mu| < \mu_c \equiv \sqrt{h_Z^2 - |\Delta_{\text{sc}}|^2}$, the system is in a topologically non-trivial phase, hosting localized MF edge modes, whereas for $|\mu| > \mu_c$ it is topologically trivial⁶⁷. For our simulations, we use input parameters, related to experiments in InSb nanowires of length $L = 1.6\mu\text{m}$ ²⁰. In particular, we choose $g = 50$, $|\Delta_{\text{sc}}| = 250\mu\text{eV}$, $\alpha = 0.02\text{eVnm}$, $m_{\text{eff}} = 0.015m_e$ and $B = 0.25\text{T}$. Also, we checked that all our results hold for different parameter variations, justifying the robustness of our calculations.

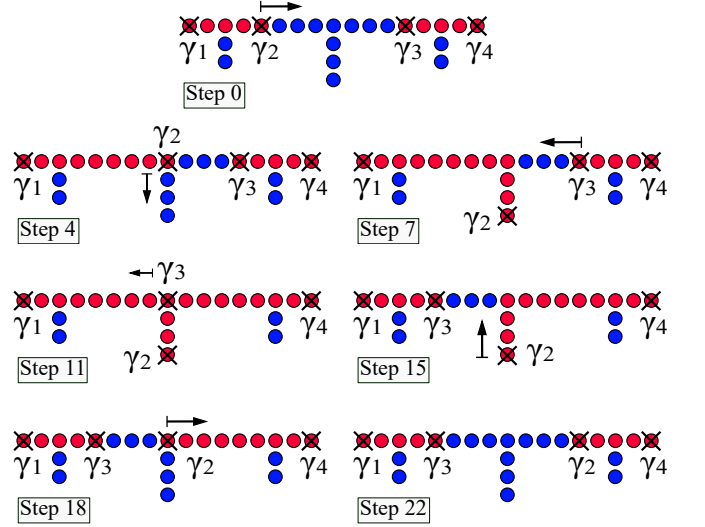


FIG. 2: Exchange protocol $\gamma_2 \leftrightarrow \gamma_3$. With $N_{\text{leg}}^t = 2$, $N_{\text{leg}}^T = 3$ and $N_{\text{gate}} = 1$ the braiding is realized in 22 exchange steps, corresponding to different keyboard gate configurations. Red (blue) regions encode topologically non-trivial (trivial) junction parts with associated Majorana modes $\gamma_{1,2,3,4}$.

Majorana single qubit states are generated by at least four MF modes. Shifting these modes spatially, enables the construction of topological gates, using their non-abelian braiding statistics.

In this work, we will analyze the exchange of MF modes in so-called **tTt** junctions, by using a common tight-binding (TB) approach with effective lattice constant a . Fig. 1, shows the structure of such a device, consisting of four connected nanowires, where **CP1**, **CP2** and **CP3** denote the three nanowire intersection points. The chemical potential on each site can be controlled independently via a "keyboard" gate. Topologically non-trivial junction parts, characterized by $\mu_{\text{nontrivial}}$, can be shifted in the topologically trivial region, by applying a certain chemical potential μ_{gate} . The device is characterized by two different stub lengths. N_{leg}^t counts the lattice points of the outer **t** structures, which are initially in the topologically non-trivial region, illustrated in red. In comparison, N_{leg}^T characterizes the geometry of the central **T** structure, which is initially in the topologically trivial phase, denoted in blue. Due to the four topological boundaries in the system, one generates in total four MF modes, encoded by $\gamma_{1,2,3,4}$. Majorana exchange processes are achieved by applying a time and site dependent potential $\mu_{\text{gate},i}(t)$. While the amount of neighbored lattice points which are shifted simultaneously, is defined by N_{gate} , $t_{\text{step}} \equiv t_j - t_{j-1}$ characterizes the time scale on which $\mu_{\text{gate},i}$ is ramped up/down in an exchange step j . The latter parameter, t_{step} , needs to be adjusted to ensure (quasi-)adiabatic braiding protocols. In particular, the chemical potential on site i in exchange step j is su-

Braiding	$\psi_1 \equiv \frac{1}{2}(\gamma_1 + i\gamma_2)$ $\psi_2 \equiv \psi_1^\dagger = \frac{1}{2}(\gamma_1 - i\gamma_2)$	$\psi_3 \equiv \frac{1}{2}(\gamma_3 + i\gamma_4)$ $\psi_4 \equiv \psi_3^\dagger = \frac{1}{2}(\gamma_3 - i\gamma_4)$	$ (\kappa_{ij}(T))_{\alpha,\beta} $	$\text{Arg} [(\kappa_{ij}(T))_{\alpha,\beta}] \left[\frac{2}{\pi} \right]$
$\gamma_1 \leftrightarrow \gamma_2$	$\psi_1 \xrightarrow{B_{12}} i\psi_1$ $\psi_2 \xrightarrow{B_{12}} -i\psi_2$	$\psi_3 \xrightarrow{B_{12}} \psi_3$ $\psi_4 \xrightarrow{B_{12}} \psi_4$	$\delta_{\alpha,\beta}$	$\begin{pmatrix} 1 & 0 & 0 & 0 \\ 0 & -1 & 0 & 0 \\ 0 & 0 & 0 & 0 \\ 0 & 0 & 0 & 0 \end{pmatrix}$
$\gamma_3 \leftrightarrow \gamma_4$	$\psi_1 \xrightarrow{B_{34}} \psi_1$ $\psi_2 \xrightarrow{B_{34}} \psi_2$	$\psi_3 \xrightarrow{B_{34}} i\psi_3$ $\psi_4 \xrightarrow{B_{34}} -i\psi_4$	$\delta_{\alpha,\beta}$	$\begin{pmatrix} 0 & 0 & 0 & 0 \\ 0 & 0 & 0 & 0 \\ 0 & 0 & 1 & 0 \\ 0 & 0 & 0 & -1 \end{pmatrix}$
$\gamma_2 \leftrightarrow \gamma_3$	$\psi_1 \xrightarrow{B_{23}} \frac{1}{2}(\gamma_1 - i\gamma_3)$ $\psi_2 \xrightarrow{B_{23}} \frac{1}{2}(\gamma_1 + i\gamma_3)$	$\psi_3 \xrightarrow{B_{23}} \frac{1}{2}(\gamma_2 + i\gamma_4)$ $\psi_4 \xrightarrow{B_{23}} \frac{1}{2}(\gamma_2 - i\gamma_4)$	$\frac{1}{2}$	$\begin{pmatrix} 0 & 0 & -1 & -1 \\ 0 & 0 & 1 & 1 \\ -1 & 1 & 0 & 2 \\ -1 & 1 & 2 & 0 \end{pmatrix}$

TABLE I: Exchange statistics of the hybridized MF states $\psi_{1,2,3,4}$, generated by the four MF modes γ_ζ ($\zeta \in \{1, 2, 3, 4\}$). The MF braiding operations are mediated by $B_{l,l+1} \equiv (1 + \gamma_l \gamma_{l+1})/\sqrt{2}$ ($l \in \{1, 2, 3\}$) and the overlap of $\psi_\beta(t=0)$ and $\psi_\alpha(T)$ with $\{\alpha, \beta\} \in \{1, 2, 3, 4\}$, is characterized by $(\kappa_{ij})_{\alpha,\beta}(T)$ (cf. Eq. (3)). Here, $\{i, j\} \in \{1, 2, 3, 4\}$ specify the MF braiding procedure¹².

perimposed by the smooth gating potential ($t \in [t_{j-1}; t_j]$)

$$\mu_{\text{gate},i}(t) = \mu_{\text{gate}} \times \begin{cases} \sin^2 \left(\frac{t - t_{j-1}}{t_{\text{step}}} \frac{\pi}{2} \right) & \text{up} \\ 1 - \sin^2 \left(\frac{t - t_{j-1}}{t_{\text{step}}} \frac{\pi}{2} \right) & \text{down} \end{cases}$$

The gating potential is kept constant (0 or μ_{gate}) in all other exchange steps. We distinguish two different types of braiding. The protocol for an exchange $\gamma_1 \leftrightarrow \gamma_2$ is visualized in Fig. 1. To obtain a closed loop, $\text{step}=12$ needs to coincide with $\text{step}=0$. The protocol for an exchange $\gamma_2 \leftrightarrow \gamma_3$ is visualized in Fig. 2. Numerically, we simulate these processes by solving the time dependent BdG equation, including the full Hamiltonian

$$\mathcal{H}_{\text{BdG}}(t) \equiv \mathcal{H}_{\text{BdG}}(t=0) + \mu_{\text{gate}}(t) \tau_3 \otimes \sigma_0. \quad (2)$$

In our system, state evolution is given by

$$\psi_i(t + \Delta t) = e^{-\frac{i}{\hbar} \mathcal{H}_{\text{BdG}}(t) \Delta t} \psi_i(t),$$

where $\Delta t \equiv t_{\text{step}}/n$, and n is the number of time discretization points^{58,68}. Initial values of this differential equation are obtained by solving $\mathcal{H}_{\text{BdG}}(t=0)$ for its eigensystem. Moreover, the energy of each state $\psi_i(t)$ is given by

$$E_i(t) = \psi_i^\dagger(t) \mathcal{H}_{\text{BdG}}(t) \psi_i(t).$$

Based on the underlying PH symmetry, these energies always come in pairs $\pm E_i(t)$. We want to emphasize, that due to the finite energy of HMF modes at $t=0$, their accumulated geometrical phase during any MF exchange process is accompanied by a dynamical one

$$\phi_{\text{dyn}}^i(t) = -\frac{1}{\hbar} \int_0^t E_i(t') dt'.$$

All dynamical phases are real, PH anti-symmetric and can be eliminated after complete MF braiding processes ($t=T$), by gauging $\psi_i(T) \rightarrow e^{-i\phi_{\text{dyn}}^i(T)} \psi_i(T)$.

III. EXCHANGE STATISTICS

The basic idea of TQC algorithms is the realization of topologically protected quantum gates, using the geometrical exchange phases of non-abelian anyons. As explained in the previous section, we realize such processes by the braiding of four Majorana fermions $\gamma_{1,2,3,4}$. Theoretically, the pairing of zero energy MFs into the associated fermionic states is arbitrary and therefore represents a choice of basis¹². However, beyond the zero energy limit, it is natural to combine two MFs to a nonlocal hybridized fermionic state (HMF mode) if they pairwise have a strong spatial overlap. Since this is the case in our finite size system, this dictates the definitions of our HMF modes $\psi_{1,2,3,4}$ in Tab. I⁶⁸. We want to remark that the two distinct topologically non-trivial regions of the tTt structure are not perfectly decoupled for $t=0$. As a consequence, the modes γ_2 and γ_3 weakly hybridize via the center T structure, which will be discussed in Sec. V.

In particular, the finite hybridization energy of the HMF modes lifts the degeneracy of a perfect Majorana system, which has two important consequences: On the one hand, it allows us to uniquely identify and determine all HMF states and their corresponding energies in each exchange step. On the other hand it defines an upper bound for our exchange time t_{step} . To realize a successful MF braiding process, t_{step} needs to be adiabatic with respect to the bulk gap, avoiding bulk excitations. At the same time, it needs to be diabatic with respect to the finite HMF hybridization gaps. Particularly, this

ensures that the HMF modes can freely rotate within their non-degenerated computational sub-space, which is a mandatory condition to obtain non-trivial exchange phases. While this requirement is absent for zero energy Majorana systems, it enforces our exchange protocols to be executed merely (quasi-)adiabatically^{66,68}.

In Tab. I, we explicitly transfer the non-abelian braiding statistics of our four Majorana states $\gamma_{1,2,3,4}$ to the exchange statistics of the corresponding HMF modes $\psi_{1,2,3,4}$, where the operators $B_{l,l+1} \equiv (1 + \gamma_l \gamma_{l+1}) / \sqrt{2}$ ($l \in \{1, 2, 3\}$) mediate the particular braiding operation¹². To check whether our simulated exchange processes provide the predicted exchange statistics, we define a time dependent quantity which calculates the overlap of states $\psi_\beta(t=0)$ and $\psi_\alpha(t)$ with $\{\alpha, \beta\} \in \{1, 2, 3, 4\}$:

$$(\kappa_{ij})_{\alpha,\beta}(t) = \langle \psi_\beta(t=0) | (B_{ij} \psi_\alpha B_{ij}^{-1})(t) \rangle, \quad (3)$$

where $\{i, j\} \in \{1, 2, 3, 4\}$ characterizes the particular type of exchange. For successful MF exchange processes, the absolute values and geometrical phases of $(\kappa_{i,j})_{\alpha,\beta}(T)$ are explicitly listed in Tab. I. In Sec. V, we will use these results to compare the simulated braiding processes with the associated theoretical predictions.

IV. BRANCHED NANOWIRE NETWORKS

Before we present our Majorana braiding results, let us discuss an effect which also has been recently predicted in Refs. 55 and 56, namely the formation of additional MF modes in networks made of very thin nanowires. Originally, Majorana modes were predicted at the topological boundaries of strictly one-dimensional p -wave wires. If the wire width does not exceed the superconducting coherence length, such modes also occur beyond the single channel limit^{69,70}. Therefore, two-dimensional junctions formed by quasi-one-dimensional nanowires smaller than the underlying superconducting coherence length are appropriate for realizing MF exchange processes. However, as numerically has been shown by the authors of Refs. 55 and 56, a naive realization of a T-junction by simply sticking together a non-trivial horizontal with a trivial vertical nanowire induces additional low-energy states besides the original MFs at the wire intersection point (cf. inset Fig. 3). In general, these additional modes are caused by the non-uniform transverse confinement specifying the junction. At the wire intersection point the local chemical potential is altered with respect to all remaining sites, due to the additional hopping contribution, connecting the nanowire network. In the small wire limit, this implies the formation of fermionic bound states, which due to the Pauli principle effectively generate new topological boundaries. Beside the numerical analysis done in Refs. 55 and 56, we will here analytically determine the parameter dependence of the sub-gap state formation, and predict a way to reverse this process by locally gating the wire intersection point. This is

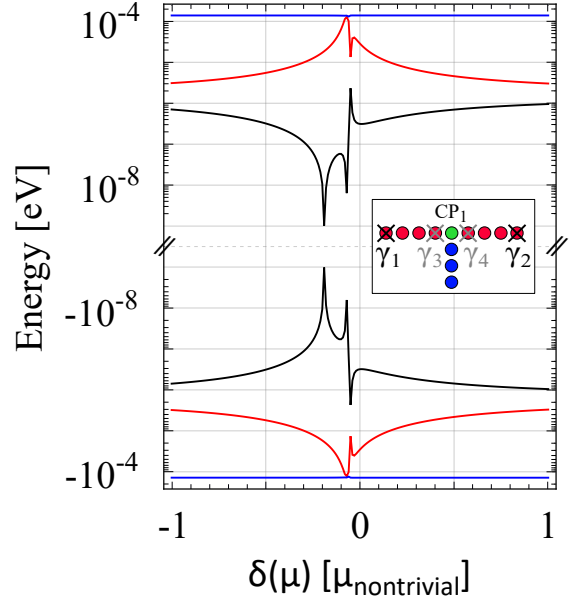


FIG. 3: The three lowest gaps of a thin t-junction, formed by a non-trivial horizontal and a trivial vertical nanowire are shown as a function of the CP_1 on-site potential $\delta\mu$. For $\delta\mu=0$, one observes the formation of additional sub-gap states, a property which can be corrected by applying $\delta\mu_{\text{corr}}$.

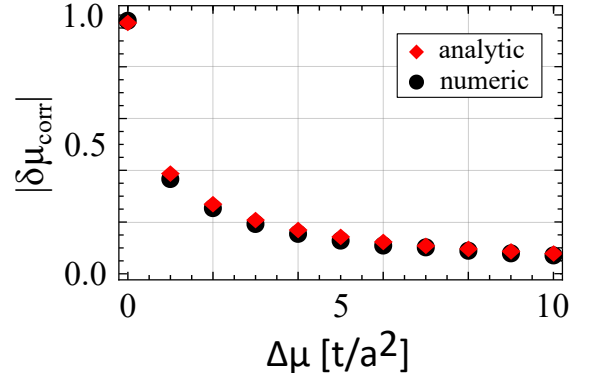


FIG. 4: Analytically and numerically determined values of $|\delta\mu_{\text{corr}}|$ as a function of $\Delta\mu$. For $\Delta\mu=0$, one exactly has to correct the additional t_{hop}/a^2 CP_1 hopping contribution.

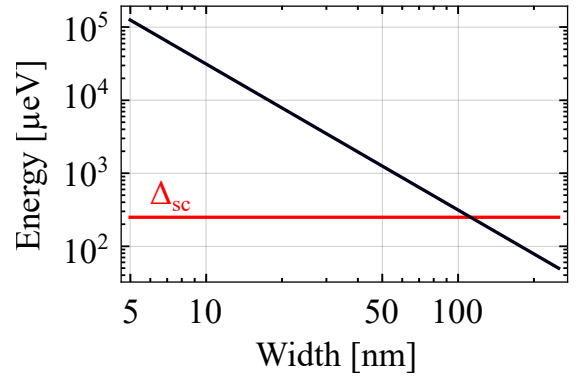


FIG. 5: Bound state energy $\Delta E_{\text{BS}}(\Delta\mu=\delta\mu=0)$ in a InSb based t-junction as a function of the wire width W . $|\Delta_{\text{sc}}|$ denotes the s -wave gap. For $W \approx 90\text{nm}$, $\Delta E_{\text{BS}}(\Delta\mu=\delta\mu=0)$ starts to exceed $|\Delta_{\text{sc}}|$, coming along with CP_1 bound states.

mandatory since any additional Majorana sub-gap state formation prohibits the exchange of the computational MF modes due to hybridization and fusing processes.

Let us explain this more carefully, considering a single t-bar junction with wire intersection point CP_1 , hopping parameter t_{hop} and lattice spacing a (cf. inset Fig. 3). The vertical (horizontal) part of this structure is topologically trivial (non-trivial), which can be achieved by implementing $\mu_{\text{nontrivial}}$ in the horizontal structure. We define the difference between chemical potentials in the two nanowires by $\Delta\mu \equiv |\mu_v - \mu_h|$ and introduce an on-site potential $V_{CP1} \equiv \delta\mu \cdot t_{\text{hop}}/a^2$ implemented at the wire intersection point. For a small lattice spacing, Fig. 3 schematically shows the three lowest energy gaps within such a t-junction as a function of $\delta\mu$. With increasing $|\delta\mu|$, one observes the formation of additional sub-gap states, indicating that the system hosts additional MF modes caused by the new topological boundaries in the junction. In particular, for small small $|\delta\mu|$ $\gamma_{1,2}$ and $\gamma_{3,4}$ form non-local fermionic states, whereas for large $|\delta\mu|$ $\gamma_{1,3}$ and $\gamma_{2,4}$ form the separate HMF modes. In the intermediate $|\delta\mu|$ all four modes hybridize, causing the characteristic energy spectrum shown in Fig. 3. Since already for $\delta\mu = 0$ the sub-states are present, even the ungated t-junction shows fermionic bound states, a property which will be enhanced if we further reduce a . Notice, that for a certain value $\delta\mu_{\text{corr}}$, the bulk energy gap can be reopened again, removing these bound states. In what follows, we determine $\delta\mu_{\text{corr}}$ analytically.

In a single, topologically non-trivial horizontal nanowire the lowest PH symmetric bulk energy is given by $\pm E_1^h = 2t_{\text{hop}}/a^2$. If $E_1^t(\Delta\mu, \delta\mu)$ denotes the corresponding energy in the full t-junction, the bound state energy is defined by $\Delta E_{\text{BS}}(\Delta\mu, \delta\mu) \equiv |E_1^h - E_1^t(\Delta\mu, \delta\mu)|$. This difference can be minimized by adjusting $\delta\mu$, allowing for a numerical scheme to determine $\delta\mu_{\text{corr}}$. Analytically, one can calculate the corresponding strength by using the single particle Green's function in the disconnected, horizontal nanowire

$$G_h^0(E) = (E - H_h)^{-1},$$

where H_h is the associated Hamiltonian. Connecting vertical and horizontal wire parts leads to an additional term in the horizontal Green's function

$$G_h^t(E) = (E - H_h - [g_v^{\text{CP1}}]^{-1}(E))^{-1} \quad (4)$$

$$[g_v^{\text{CP1}}]^{-1}(E) = \sum_{n,v} \frac{\langle \text{CP1} | H_{\text{hop}} | n, v \rangle \langle n, v | H_{\text{hop}} | \text{CP1} \rangle}{E - E_{n,v}}.$$

Here $|n, v\rangle$ denotes a state $|n\rangle$ in the vertical wire and H_{hop} represents the hopping matrix, connecting the t-junction. Hence, $(g_v^{\text{CP1}})^{-1}(E)$ describes the additional hopping from the horizontal into the vertical wire and back ($\mathcal{O}(t_{\text{hop}}^2)$). Hence, it resembles the inverse of the local, vertical Green's function. According to Eq. (4), We can exactly reverse the formation of bound states at site CP_1 , if we choose $V_{\text{CP1}}^{\text{corr}} = (g_v^{\text{CP1}})^{-1}(E_1^h)$.

Fig. 4 shows numerically and analytically determined values of $\delta\mu_{\text{corr}}$ as a function of $\Delta\mu$, which perfectly match each other. With increasing $\Delta\mu$, hoppings from the horizontal into the vertical wire get more and more unfavorable, leading to a rapid decrease of $\delta\mu_{\text{corr}}$. Notice, that for $\Delta\mu = 0$, we obtain $\delta\mu_{\text{corr}} = 1$, correcting the single, additional hopping term at CP_1 .

As explained in the beginning of this section, narrow, quasi-one dimensional channels are required to observe Majorana bound states in T-junctions. We proved that in such systems additional MF modes may occur at wire intersection points, requiring for a correction potential. Let us close this section by discussing the experimental relevance of this effect. For our set of parameters (cf. Sec. II), the competing energy scales are given by⁷¹⁻⁷³:

$$\Delta E_{\text{BS}}(\Delta\mu = \delta\mu = 0) \approx \frac{1}{8} \left(\frac{\pi}{W} \right)^2 \frac{\hbar^2}{2m^*}$$

$$E_{\text{SO}} = \frac{\alpha^2 m^*}{(2\hbar)^2} \approx 50 \mu\text{eV} \quad \wedge \quad |\Delta_{\text{sc}}| \approx 250 \mu\text{eV}$$

Fig. 5 shows $\Delta E_{\text{BS}}(\Delta\mu = \delta\mu = 0)$ as a function of the wire width. A perceivable fermionic bound state formation is expected to be present as soon as $\Delta E_{\text{BS}}(\Delta\mu = \delta\mu = 0)$ exceeds $|\Delta_{\text{sc}}|$, which happens for $W \lesssim 100\text{nm}$. However, the associated formation of extra topological boundaries and correspondingly the formation of additional MF modes in the system rather occurs for smaller values of W , since this requires a strong localization of the fermionic CP_1 bound states. Numerically, we observe this process for $W < 30\text{nm}$, which corresponds to $\Delta E_{\text{BS}}(\Delta\mu = \delta\mu = 0) > 10 |\Delta_{\text{sc}}|$. Nevertheless, we want to emphasize that due to $\Delta E_{\text{BS}}(\Delta\mu \neq \delta\mu = 0) \ll \Delta E_{\text{BS}}(\Delta\mu = \delta\mu = 0)$, this critical width decreases for $\Delta\mu \neq 0$, which is a mandatory requirement for all TQC algorithms. Therefore, even though we expect additional HMF modes in ungated, experimental TQC networks made of InSb nanowires of width $W \approx 75\text{nm}$ ²⁰, we predict that such modes do not occur for our MF braiding operations due to the gating potential.

V. BRAIDING SIMULATIONS

First, we analyze the braiding process $\gamma_1 \leftrightarrow \gamma_2$, using the exchange protocol, defined in Fig. 1. We executed our simulations for various stub lengths $L_{\text{leg}}^{\text{T}} = aN_{\text{leg}}^{\text{T}}$ and $L_{\text{leg}}^{\text{t}} = aN_{\text{leg}}^{\text{t}}$, characterizing different geometries of our tTt-setup (cf. setup Fig.1), as well as for different gating times t_{step} . Each of these parameters has a different effect on the braiding, which we separately discuss in the following.

In Fig. 6a, we illustrate $(\kappa_{12}(T))_{11}$ as a function of $L_{\text{leg}}^{\text{t}}$, whereas t_{step} and $L_{\text{leg}}^{\text{T}}$ are chosen appropriately. To ensure a successful braiding procedure, we need to satisfy $\Delta_{\text{hyb}}(\gamma_1, \gamma_2) \ll |\Delta_{\text{sc}}|$ throughout the entire exchange process, which can be achieved by keeping the MF modes

separated in space. For our set of parameters $L_{\text{leg}}^t > 2\mu\text{m}$ fulfills this condition, implying the predicted geometrical exchange phase of $\pi/2$ (cf. Tab. I). Let us clarify the effect of L_{leg}^T on the exchange procedure $\gamma_1 \leftrightarrow \gamma_2$. The braiding statistics in Tab. I was evaluated for the HMF basis vectors $\psi_{1,2,3,4}$. Explicitly, we assumed that the MF modes $\gamma_{1,2}$, as well as $\gamma_{3,4}$ hybridize to the associated HMF states. If the hybridization between $\gamma_{1,2}$ as well as between $\gamma_{3,4}$ initially (finally) is much stronger than the hybridization between $\gamma_{2,3}$, this is the proper description of our tTt structure at $t=0$ ($t=T$). In general, this can be guaranteed either by choosing $L_{\text{leg}}^T \gg L_{\text{leg}}^t$ or by initially (finally) applying a strong gating potential $\mu_{\text{trivial}} = \mu_{\text{gate}} + \mu_{\text{nontrivial}}$, acting as a potential barrier in the central T structure⁷⁴. We found that quantitatively this requirement corresponds to

$$\frac{\Delta_{\text{hyb}}(\gamma_1, \gamma_2)}{\Delta_{\text{hyb}}(\gamma_2, \gamma_3)} = \frac{e^{-2L_{\text{leg}}^t}}{e^{-2L_{\text{leg}}^T} \times \left(\frac{\mu_{\text{trivial}}}{\mu_{\text{nontrivial}}}\right)^{-2L_{\text{leg}}^T}} \gg 1$$

$$\Rightarrow L_{\text{leg}}^T \gg L_{\text{leg}}^t \left(1 + \ln \left[\frac{\mu_{\text{trivial}}}{\mu_{\text{nontrivial}}}\right]\right)^{-1}. \quad (5)$$

Next, we specify requirements on t_{step} for a successful exchange process $\gamma_1 \leftrightarrow \gamma_2$ numerically as well as analytically. In Figs. 6b-c, $|(\kappa_{12}(T))_{11}|$ and $\text{Arg}[(\kappa_{12}(T))_{11}]$ are shown as a function of t_{step} for several values of $L_{\text{leg}}^T \geq L_{\text{leg}}^t = L_{\text{gate}}$. For large values of t_{step} , all $\kappa_{12}(T)$ matrix elements approximate their theoretical predictions (cf. Tab. I). In particular, we identify $t_{\text{step}}^{\text{qad}} \approx 6.5\text{ns}$ to be the fastest, (quasi-)adiabatic gating time. As introduced and discussed in Sec. I, the (quasi-)adiabatic time scale $t_{\text{step}}^{\text{qad}}$ defines the scale beyond which MF modes do not mix or scatter with bulk states, but are still able to freely rotate within their non-degenerated computational subspace. With $\text{gate} = L_{\text{leg}}^t$, our braiding protocol $\gamma_1 \leftrightarrow \gamma_2$ is related to six exchange steps. This leads to a minimal (quasi-)adiabatic braiding time of $T_{\text{qad}}(\gamma_1 \leftrightarrow \gamma_2) \approx 40\text{ ns}$. Let us analytically derive this lower boundary. In general, the adiabatic theorem of quantum mechanics predicts an adiabatic time evolution of a state $|n(t)\rangle$ with energy $E_n(t)$, if $(\forall m \neq n \wedge \forall t)$ ^{75,76}

$$\left| \left\langle m(t) \left| \frac{\partial \hat{H}(t)}{\partial t} \right| n(t) \right\rangle \right| \ll \hbar^{-1} |E_m(t) - E_n(t)|^2. \quad (6)$$

Let us assume that $|n(t)\rangle$ defines a HMF mode, scattering with bulk modes $|m(t)\rangle$ in the non (quasi-)adiabatic limit. The time dependent, TB scattering matrix $\hat{H}(t)$ can be evaluated, using Eq. (2). For $N_{\text{gate}} = 1$, this matrix only has one nonzero entry related to lattice site i , if the gating potential is solely varied at this point in the j -th exchange step ($t \in [t_{j-1}; t_j]$):

$$\frac{\partial H_{ii}(t)}{\partial t} = \frac{\pi \mu_{\text{gate}}}{t_{\text{step}}} \sin \left[\frac{\pi(t-t_{j-1})}{2t_{\text{step}}} \right] \cos \left[\frac{\pi(t-t_{j-1})}{2t_{\text{step}}} \right]. \quad (7)$$

In general, Eq. (6) needs to be valid for all exchange times. To determine an explicit (quasi-)adiabatic boundary for t_{step} , we therefore need to derive the maximum value of $|\langle m(t) | [\partial_t \hat{H}(t)] | n(t) \rangle|$. With the maximum of Eq. (7) and due to the fact that the HMF modes exactly peak at site $i \rightarrow i+1$ in the corresponding exchange step, we obtain

$$\max \left[\left\langle m(t) \left| \frac{\partial \hat{H}(t)}{\partial t} \right| n(t) \right\rangle \right] = \frac{\pi \mu_{\text{gate}}}{2 t_{\text{step}}} \max [{}_i \langle m(t) | n(t) \rangle] = \frac{\pi \mu_{\text{gate}}}{2 t_{\text{step}}}. \quad (8)$$

Therefore, Eqs. (6)-(8) imply $(|E_m(t) - E_n(t)| \approx |\Delta_{\text{sc}}|)$:

$$\frac{\mu_{\text{gate}}}{t_{\text{step}}} \ll \hbar^{-1} |\Delta_{\text{sc}}|^2. \quad (9)$$

If we fix $|\Delta_{\text{sc}}|$, Eq. (9) predicts a (quasi-)adiabatic exchange process either for large t_{step} , or rather for small μ_{gate} , which we confirmed numerically. For a fast exchange, one therefore needs to choose a small gating potential, which is still able to shift topological boundaries. Notice that Eq. (9) satisfies the common and intuitive condition $t_{\text{step}} \ll |\Delta_{\text{sc}}|^{-1}$. However, for the first time, it also explicitly takes into account the rate with which the gating potential μ_{gate} is ramped up/down. It is therefore much more accurate than all common qualitative estimations of (quasi-)adiabatic gating times in literature^{59,68}. Let us analyze the exchange $\gamma_2 \leftrightarrow \gamma_3$, using the protocol defined in Fig. 2. These simulations were executed as a function of t_{step} and L_{leg}^T with $L_{\text{gate}} = L_{\text{leg}}^t = 3\mu\text{m}$.

To check the braiding statistics, given in Tab. I, we introduce a new, simplified quantity. For a successful exchange process $\gamma_2 \leftrightarrow \gamma_3$, any matrix element of $|\kappa_{23}(T)|$ is $\pi/2$. Thus, we define the average value

$$\overline{\text{abs}}(T) \equiv \sum_{\{\alpha, \beta\} \in \{1,2,3,4\}} \frac{1}{16} \times |(\kappa_{23}(T))_{\alpha, \beta}|,$$

also counting $\pi/2$ for successful exchange processes of this kind. Fig. 6d, shows $\overline{\text{abs}}(T)$ as well as $\text{Arg}[(\kappa_{23}(T))_{\alpha, \beta}]$ as a function of t_{step} for $L_{\text{leg}}^T = 2L_{\text{leg}}^t$. One clearly determines (quasi-)adiabatic exchange processes for $t_{\text{step}} \gtrsim 4\text{ns}$, perfectly agreeing with Eq. (9). We also checked that all single constituents of $\overline{\text{abs}}(T)$ show the same feature. In comparison to $\gamma_1 \leftrightarrow \gamma_2$, the present exchange process comes along with a slightly smaller $t_{\text{step}}^{\text{qad}}$, resulting from slightly smaller HMF hybridization energies. In contrast to the first process, with $\text{gate} = L_{\text{leg}}^t$ the current braiding is related to 14 exchange steps, which leads to a minimal, (quasi-)adiabatic braiding time of $T_{\text{qad}}(\gamma_2 \leftrightarrow \gamma_3) \approx 55\text{ns}$.

We close this section by discussing the upper, adiabatic boundary $t_{\text{step}}^{\text{ad}}$ for successful MF exchange processes. As introduced in Sec. III, this exchange time defines the scale above which all states, including HMF

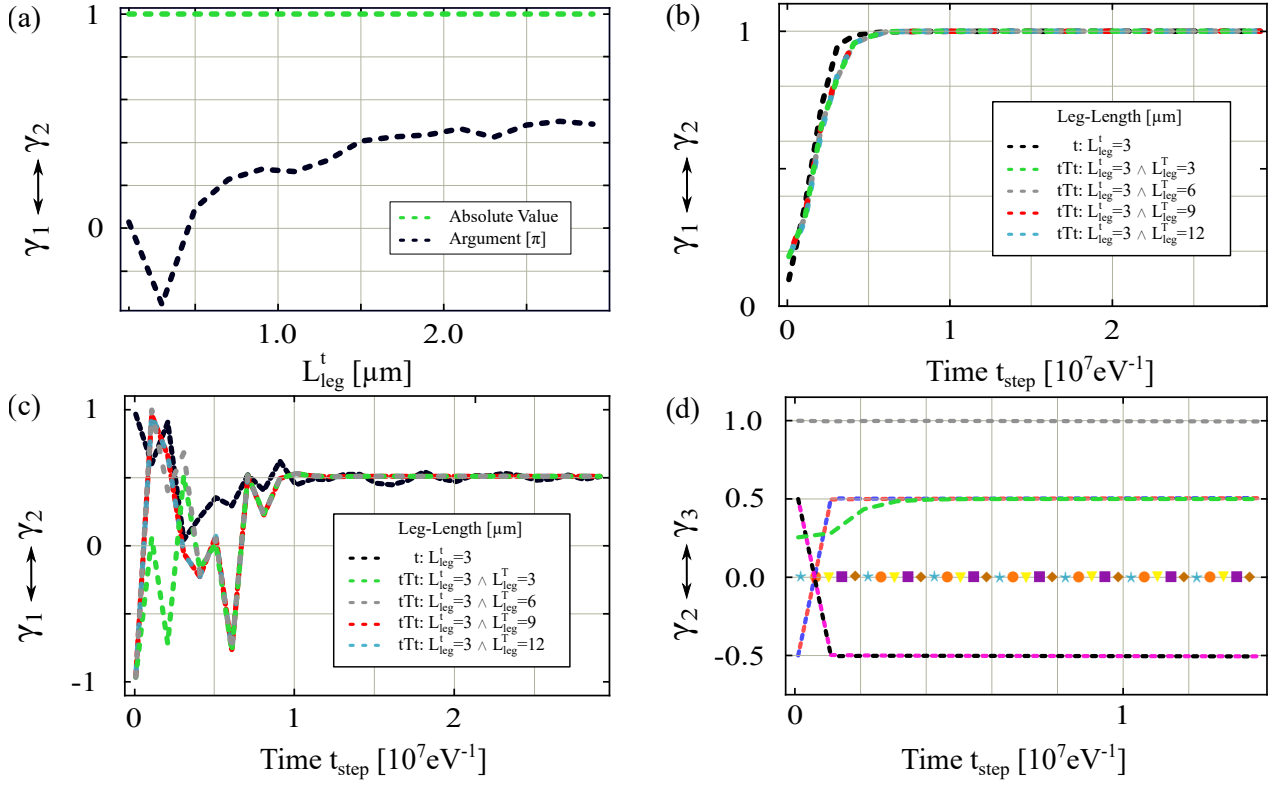


FIG. 6: (a) Absolute value and argument of $(\kappa_{12}(T))_{11}$ as a function of L_{leg}^t for an (quasi-)adiabatic braiding $\gamma_1 \leftrightarrow \gamma_2$ with $L_{\text{Gate}} = L_{\text{leg}}^t$ and $L_{\text{leg}}^T = 6\mu\text{m}$. With increasing L_{leg}^t , $\text{Arg}[(\kappa_{12}(T))_{11}]$ approximates the theoretical prediction of $\pi/2$. (b) $|(\kappa_{12}(T))_{11}|$ & (c) $\text{Arg}[(\kappa_{12}(T))_{11}]$ $[\pi]$ as a function of t_{step} for several values $L_{\text{leg}}^T \geq L_{\text{leg}}^t = L_{\text{Gate}}$. For all geometries and large t_{step} both quantities approximate their theoretical prediction. In the limit of small t_{step} , non (quasi-)adiabatic effects lead to deviations from this limit. (d) $\overline{\text{abs}}(T)$ & $\text{Arg}[(\kappa_{23}(T))_{\alpha,\beta}]$ $[\pi]$ with $\{\alpha, \beta\} \in \{1, 2, 3, 4\}$ are shown as a function of t_{step} for $L_{\text{leg}}^T = 2L_{\text{leg}}^t = 2L_{\text{gate}} = 6\mu\text{m}$. The curves $\text{Arg}[(\kappa_{12}(t_{\text{step}}))_{\alpha,\beta}]$ $[\pi]$, denoted in the form $(\alpha, \beta, \text{color})$, are given by (1,1,orange,●), (2,2,brown,◆), (3,3,lightblue,★), (4,4,yellow,▼), (1,2,purple,■), (1,3,black), (2,3,red), (1,4,pink), (2,4,blue) and (3,4,gray). The average value $\overline{\text{abs}}(T)$ is shown in green. In the (quasi-)adiabatic regime all quantities approximate their theoretical prediction.

modes, completely evolve adiabatically. For successful, (quasi-)adiabatic processes with $t_{\text{step}}^{\text{qad}} \ll t \ll t_{\text{step}}^{\text{ad}}$, all HMF modes are allowed to rotate in the low energy computational subspace, while bulk excitations are effectively suppressed. In contrast, for $t_{\text{step}} > t_{\text{step}}^{\text{ad}}$, these rotations are forbidden since all states purely evolve adiabatically^{66,68}. Quantitatively, an exchange $\gamma_i \leftrightarrow \gamma_j$ is realized (quasi-)adiabatically if (cf. Eq. (9))

$$t_{\text{step}} \ll \frac{\hbar \mu_{\text{gate}}}{\Delta_{\text{hyb}}^2(\gamma_i, \gamma_j)}. \quad (10)$$

For our system $t_{\text{step}}^{\text{ad}} \approx 10^5 \text{s}$. Thus, $t_{\text{step}} \ll t_{\text{step}}^{\text{ad}}$ is experimentally easy accessible.

VI. TOPOLOGICAL QUANTUM COMPUTING

In this section, we will pedagogically derive how to realize universal TQC algorithms on our tTt structures. We start the discussion by defining a logical single qubit state in the even parity subspace, formed by the four MF

modes $\gamma_{1,2,3,4}$ (cf. Tab.I)

$$|\tilde{0}\rangle \equiv \psi_1 \psi_3 |00\rangle = |00\rangle \quad \wedge \quad |\tilde{1}\rangle \equiv \psi_1^\dagger \psi_3^\dagger |00\rangle = |11\rangle. \quad (11)$$

To understand the following remarks, let us introduce some important mathematical group structures. For an n -qubit system, the Pauli group \mathcal{P}_n is defined to be⁷⁷

$$\mathcal{P}_n \equiv \{\pm i^{0,1} (\sigma_1 \otimes \dots \otimes \sigma_n) | \sigma_i \in \{\sigma_0, \sigma_x, \sigma_y, \sigma_z\}\},$$

where \mathcal{P}_1 is generated by σ_x, σ_z and $i\sigma_0$. Explicitly, this is characterized by $\mathcal{P}_1 = \langle \sigma_x, \sigma_z, i\sigma_0 \rangle$. Moreover, the group $\mathcal{P}_n = \mathcal{P}_1^{\otimes n} \equiv \mathcal{P}_1 \otimes \dots \otimes \mathcal{P}_1$ is a subgroup of the n -qubit Clifford group \mathcal{C}_n , which itself is generated by three characteristic operators:⁷⁸

$$\mathcal{C}_n \equiv \langle H_i, K_i, \Lambda(\sigma_x)_{ij} \rangle \setminus U(1).$$

In the basis $(|\tilde{0}\rangle, |\tilde{1}\rangle)$, one defines:

$$H \equiv \frac{1}{\sqrt{2}} \begin{pmatrix} 1 & 1 \\ 1 & -1 \end{pmatrix} \quad \wedge \quad K \equiv \begin{pmatrix} 1 & 0 \\ 0 & i \end{pmatrix} \quad \wedge \quad \Lambda(\sigma_x) \equiv \begin{pmatrix} I & 0 \\ 0 & \sigma_x \end{pmatrix},$$

where H represents the (single qubit i) Hadamard gate, K denotes the (single qubit i) phase shift gate and $\Lambda(\sigma_x)$ resembles the (two qubit (i, j)) **Controlled NOT** gate. Since $\mathcal{P}_1 \subset \mathcal{C}_1$, Pauli gates can be constructed via⁷⁸:

$$\sigma_z = K^2, \sigma_x = HK^2H, \sigma_y = -\frac{i}{2}[\sigma_x, \sigma_y].$$

Next, we introduce the Gottesman-Knill theorem, stating that quantum computation schemes built on the following requirements are realizable in polynomial time on a probabilistic, classical computer⁷⁹:

- (I) Initialization of computational $|\tilde{0}\rangle$
- (II) Realization of \mathcal{C}_n operations
- (III) Readout of \mathcal{P}_n operators
- (IV) Classical control, conditioned on (III).

We define $\mathcal{O}_{\text{ideal}}$ to be the set of all algorithms based on this protocol⁷⁸. Since \mathcal{C}_n alone does not represent a universal set of quantum gates, we extend \mathcal{C}_n by another independent gate, ensuring this property⁸⁰. For TQC algorithms it is convenient to extend \mathcal{C}_n by the single qubit, $\pi/8$ phase gate^{81,82}

$$T \equiv \begin{pmatrix} 1 & 0 \\ 0 & e^{i\pi/4} \end{pmatrix}.$$

Up to overall phases, one can rewrite the MF braiding operators B_{ij} (cf. Tab. I) in the even parity subspace via

$$B_{1,2} = B_{3,4} = e^{-i\pi/4} \begin{pmatrix} 1 & 0 \\ 0 & i \end{pmatrix} \wedge B_{2,3} = \frac{1}{\sqrt{2}} \begin{pmatrix} 1 & -i \\ -i & 1 \end{pmatrix}.$$

Thus, up to overall phases, we are able to construct the phase shift and Hadamard gate via consecutive braiding operations⁸³:

$$K = B_{12} = B_{34} \quad \wedge \quad H = B_{1,2}B_{2,3}B_{1,2}.$$

Hence, based on the Majorana braiding times in Sec. V, we can realize the phase gate on the order of $\mathcal{O}(10\text{ns})$ and the Hadamard gate on the order of $\mathcal{O}(10^2\text{ns})$. To build the $\Lambda(\sigma_x)$ gate, we have to define a two qubit system, containing at least eight MF states $\gamma_{1,2,\dots,8}$. In the even parity subspace, general two qubit states read

$$|\Psi\rangle = a|\tilde{0}, \tilde{0}\rangle + b|\tilde{0}, \tilde{1}\rangle + c|\tilde{1}, \tilde{0}\rangle + d|\tilde{1}, \tilde{1}\rangle,$$

with $(a, b, c, d) \in \mathbb{C}$. Such a system can be defined on two adjacent tTt structures, where the first (second) qubit is characterized by $\gamma_{1,2,3,4}$ ($\gamma_{5,6,7,8}$). However, if MF braiding processes are the only present computational operations, an arbitrary two qubit state can always be written as a single qubit product state

$$|\Psi\rangle = |\Psi_1\rangle \otimes |\Psi_2\rangle,$$

known as the no-entanglement rule. Hence, the construction of entangled (Bell) states is not possible by MF

braiding operations alone⁸⁰. This is a central problem of Majorana based TQC and justifies the requirement of projective measurements. We will prove this statement, using the stabilizer formalism⁸⁴. Therefore, we define an abelian subgroup $S_{|\psi\rangle} \equiv \langle g_1, \dots, g_n \rangle \subset P_n$, generated by n -commuting and independent elements $g_i \in P_n$, such that $-\sigma^{\otimes n} \notin S_{|\psi\rangle}$. This group is called stabilizer and uniquely defines an n -qubit $+1$ eigenstate $|\psi\rangle$ via^{77,85}

$$g_i|\psi\rangle = |\psi\rangle \quad \forall \quad g_i \in S_{|\psi\rangle} \quad \wedge \quad i \in \{1, 2, \dots, n\}. \quad (12)$$

For TQC codes, we define a vector space V_S of dimension 2^k , such that V_S is stabilized by $S = \langle g_1, \dots, g_{n-k} \rangle$ ^{77,84}. If one applies a unitary operation U to V_S , one obtains

$$U|\psi\rangle = Ug|\psi\rangle = UgU^\dagger U|\psi\rangle$$

for any $|\psi\rangle \in V_S$ and $g \in S$ ⁷⁷. Hence, the vector space $V'_S \equiv UV_S$ is stabilized by $S' \equiv \{UgU^\dagger | g \in S\}$. We are now in the position to prove the no-entanglement rule. Therefore, we consider an initial two qubit state $|\psi\rangle = |\tilde{0}, \tilde{0}\rangle$, characterized by (up to factors $\pm 1, \pm i$)⁸⁰

$$S_{|\psi\rangle} = (\gamma_1\gamma_2, \gamma_3\gamma_4, \gamma_5\gamma_6, \gamma_7\gamma_8).$$

Applying a set of topological braiding gates, leads to

$$S_{|\psi\rangle'} = (\gamma_{p(1)}\gamma_{p(2)}, \gamma_{p(3)}\gamma_{p(4)}, \gamma_{p(5)}\gamma_{p(6)}, \gamma_{p(7)}\gamma_{p(8)}),$$

where $p(i) \in \{1, 2, \dots, 8\}$. According to Eq. (12), the two qubit state $|\psi\rangle'$ has to satisfy

$$\begin{aligned} \gamma_{p(1)}\gamma_{p(2)}|\psi\rangle' &= |\psi\rangle' & \wedge & \quad \gamma_{p(3)}\gamma_{p(4)}|\psi\rangle' = |\psi\rangle' \\ \gamma_{p(5)}\gamma_{p(6)}|\psi\rangle' &= |\psi\rangle' & \wedge & \quad \gamma_{p(7)}\gamma_{p(8)}|\psi\rangle' = |\psi\rangle'. \end{aligned}$$

Moreover, our even parity construction implies⁸⁰

$$-\gamma_1\gamma_2\gamma_3\gamma_4|\psi\rangle' = -\gamma_5\gamma_6\gamma_7\gamma_8|\psi\rangle'.$$

To fulfill all these equations, one obtains for $1 \leq j \leq 4$:

$$\begin{aligned} p(2j-1), p(2j) &\in \{1, 2, 3, 4\} \\ \vee \quad p(2j-1), p(2j) &\in \{5, 6, 7, 8\}. \end{aligned}$$

Hence, each $g \in S_{|\psi\rangle'}$ is either bilinear in $\gamma_{1,2,3,4}$ or $\gamma_{5,6,7,8}$, which implies the product structure of $|\psi\rangle'$ ⁸⁰.

To circumvent the no-entanglement rule, we will use the concept of so-called projective measurements, which will enable entanglement between topological (Majorana) qubits and therefore allow the realization of CNOT gates. To understand how this comes about, let us consider that our system is defined by an n -qubit state $|\psi\rangle$, stabilized by $S_{|\psi\rangle} = \langle g_1, \dots, g_n \rangle$. Further, we assume that one wants to measure an operator $g \in \mathcal{P}_n$. Without loss of generality we define g to be a pure tensor product of Pauli matrices. After measuring g , the stabilizer $S_{|\psi\rangle}$ needs to be updated, leading to two different scenarios⁷⁷:

- (I) $\forall i \in \{1, \dots, n\}$: $[g, g_i] = 0$.

- (II) $\exists i \in \{1, \dots, n\}$, such that $\{g, g_i\}_+ = 0$.
 Without loss of generality: $[g, g_j] = 0$
 for $j \in \{2, \dots, n\}$ and $\{g, g_1\}_+ = 0$.

In case (I), either g or $-g$ needs to be an element of $S_{|\psi\rangle}$. This is based on the fact that $g_i g |\psi\rangle = g g_i |\psi\rangle = g |\psi\rangle$ and $g^2 = \sigma_0^{\otimes n}$ for all $i \in \{1, \dots, n\}$, implying $g |\psi\rangle = \pm |\psi\rangle$. Let us assume that $g \in S_{|\psi\rangle}$. In general, after measuring g with outcome λ , the n -qubit state $|\psi\rangle$ needs to be multiplied by the projection operator

$$\Pi_\lambda = \frac{1}{2} (\sigma_0^{\otimes n} + \lambda g).$$

For $g \in S_{|\psi\rangle}$, $\lambda = 1$ and $\Pi_1 = \sigma_0^{\otimes n}$. Thus in scenario (I), measuring g does not effect $S_{|\psi\rangle}$ ⁷⁷. Such processes can not generate any entanglement in the system. In scenario (II), the situation differs. This time, $\Pi_{\pm 1}$ dictates the measurement probabilities

$$p(\pm 1) = \text{Tr} \left(\frac{1 \pm g}{2} |\psi\rangle\langle\psi| \right) = \text{Tr} \left(g_1 \frac{1 \mp g}{2} |\psi\rangle\langle\psi| \right),$$

where we used $g_1 |\psi\rangle = |\psi\rangle$ and $g g_1 = -g_1 g$. With the cyclic property of the trace and with $g_1 = g_1^\dagger$, one obtains $p(1) = p(-1)$. Due to $p(1) + p(-1) = 1$, one finally gets $p(\pm 1) = 1/2$. After measuring g with outcome $\lambda = \pm 1$, the projected states are given by⁷⁷

$$|\psi^{\pm 1}\rangle = \frac{\sigma_0^{\otimes n} \pm g}{\sqrt{2}} |\psi\rangle \quad \text{with} \quad S_{|\psi^{\pm 1}\rangle} = \langle \pm g, g_2, \dots, g_n \rangle.$$

Thus, in scenario (II), g_1 is replaced by $\pm g$ in $S_{|\psi^{\pm 1}\rangle}$. This enables the addition of operator combinations $\gamma_{1,2,3,4} \gamma_{5,6,7,8}$ to the updated stabilizer, such that $S_{|\psi^{\pm 1}\rangle}$ eventually defines an entangled (Bell) state.

Inspired by this idea, the first Majorana based CNOT gate was proposed by S. Bravyi and A. Kitaev in Refs. [78, 80, 86]. Their concrete gate realization relies on nondestructive parity measurements of ancillary MF states and long-range MF braiding operations. For our tTt building blocks, we choose a slightly different CNOT gate structure, which was first suggested for $\nu = 5/2$ Ising anyons in Ref. 87 and has the advantage of strictly involving short-range MF braiding procedures. As a consequence, each MF mode stays in its initial tTt building block during all quantum operations, which is much easier to realize technically. Moreover, this setup is accompanied by smaller computation times in comparison to long-range based algorithms. In particular, Fig. 7 illustrates how to realize a CNOT gate on our nanowire based structure and explicitly shows the world lines of all involved MF modes. Explicitly, we insert a single tTt building block, hosting the four ancillary MF modes $\gamma_{5,6,7,8}$, between two tTt building blocks, which define the logical qubits. If **c**, **t** and **a** encode the control, target and ancillary qubit, our CNOT gate is given by

$$\Lambda(\sigma_x) \equiv \Pi_{p_3}^{(2)}(5, 6) \times H_a \times H_t \times \Pi_{p_2}^{(4)}(7, 8, 9, 10) \quad (13)$$

$$\times H_a \times H_t \times \Pi_{p_1}^{(4)}(3, 4, 5, 6). \quad (14)$$

Here $p_{1,2,3} = \pm 1$ represent measurement results and $H_{c,t,a}$ encode single qubit Hadamard gates. We use the following initial ancillary qubit configuration and the associated projectors of nondestructive measurements:

$$(\gamma_5 + i\gamma_6) |\psi\rangle = 0 \quad \Pi_{p_i}^{(2)}(p, q) = \frac{1}{2} (1 - ip_i \gamma_p \gamma_q)$$

$$(\gamma_7 + i\gamma_8) |\psi\rangle = 0 \quad \Pi_{p_i}^{(4)}(p, q, r, s) = \frac{1}{2} (1 + ip_i \gamma_p \gamma_q \gamma_r \gamma_s)$$

In particular, after initializing our qubits we act with a non-destructive parity measurement on the four MF modes $\gamma_{3,4,5,6}$. After that, we apply a Hadamard gate on the target and the ancilla qubit, respectively. Subsequently we non-destructively measure the parity of $\gamma_{7,8,9,10}$ followed by the application of another set of Hadamard gates acting on the ancilla and target qubit. Finally, we non-destructively measure the parity of the MF modes $\gamma_{5,6}$, which completes the protocol of our tTt-based CNOT gate.

Last, let us discuss how to construct $\pi/8$ phase gates for tTt building blocks. Such operations can be realized by using ancillary $|a_4\rangle \equiv (|\tilde{0}\rangle + e^{i\pi/4} |\tilde{1}\rangle) / \sqrt{2}$ states^{46,80}. While it is not possible to initialize these states topologically, we are able to construct so-called "noisy" copies of $|a_4\rangle$ on our tTt structures, as shown in Fig. 8. The initialization algorithm works as follows: We start with a single qubit state $|\tilde{0}\rangle$, defined by the two MF pairs $\gamma_{1,2}$ and $\gamma_{3,4}$. Then, via braiding processes, we bring γ_1 and $\gamma_3 \rightarrow -\gamma_2$ sufficiently close to each other and afterwards let the system freely evolve for a certain time τ . Eventually, we spatially separate γ_1 and γ_2 again. Let us analyze this construction scheme in detail. After the initial MF braiding operations, our system evolves to

$$|\Phi\rangle \equiv B_{1,2}^\dagger B_{2,3} |\tilde{0}\rangle = \frac{1}{\sqrt{2}} (|\tilde{0}\rangle + |\tilde{1}\rangle).$$

During the time τ , the short-range interaction between MF states is described by the following Hamiltonian, which is constructed such that it commutes with all MF parity operators⁸⁰:

$$H_{\text{int}} \equiv -i\gamma_1 \gamma_2 \otimes X + \sigma_0 \otimes Y.$$

Here, X and Y are operators acting on the environment, which initially are given by $|\Psi_E\rangle$. Their explicit form is unimportant for our line of reasoning, as will be clarified in the following. Since $-i\gamma_1 \gamma_2$ stabilizes $|\tilde{0}\rangle$, our final state (including the environment) is given by

$$|\Phi\rangle \otimes |\Psi_E\rangle = \frac{1}{\sqrt{2}} \left(|\tilde{0}\rangle \otimes e^{i(X+Y)\tau} |\Psi_E\rangle + |\tilde{1}\rangle \otimes e^{i(-X+Y)\tau} |\Psi_E\rangle \right).$$

Subsequently tracing over $|\Psi_E\rangle$ leads to a mixed state, described by the full density matrix⁸⁰

$$\rho \equiv \frac{1}{2} \begin{pmatrix} 1 & r \\ r^* & 1 \end{pmatrix} \quad \text{with} \quad r \equiv \langle \Psi_E | e^{i(X+Y)\tau} e^{i(X-Y)\tau} | \Psi_E \rangle.$$

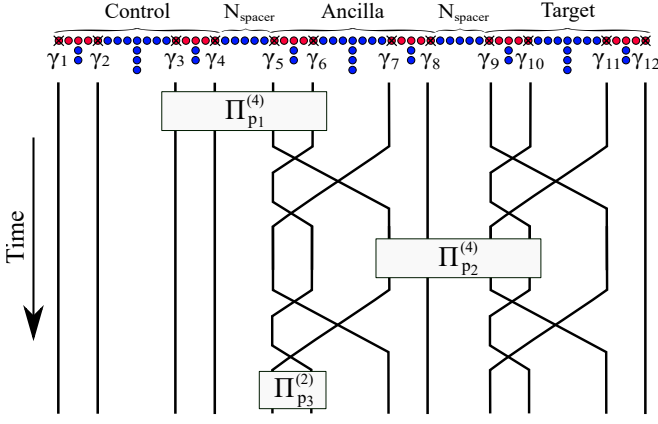


FIG. 7: Hardware setup of a CNOT gate. We show the world lines of all MF modes during this operation⁸⁷. Between the two outer tTt building blocks, defining the logical qubits by their MF modes $\gamma_{1,2,3,4}$ and $\gamma_{9,10,11,12}$, one has to implement another tTt building block, hosting the ancillary MF modes $\gamma_{5,6,7,8}$. Blue sites indicate topologically trivial, whereas red ones encode topologically non-trivial regions. The single tTt junctions are separated by N_{spacer} lattice sites, satisfying Eq. (5). $\Pi_{1,2,3}$ represent non-destructive parity measurements with outcome $p_{1,2,3}$.

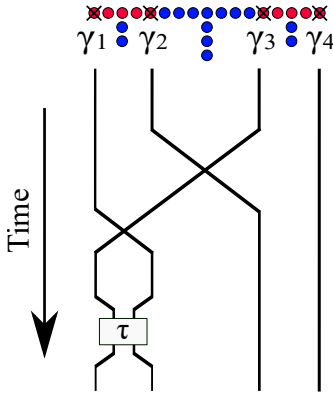


FIG. 8: Preparation of a "noisy" copy of $|a_4\rangle$, based on the short-range interaction of two MF modes during the time τ ⁸⁰.

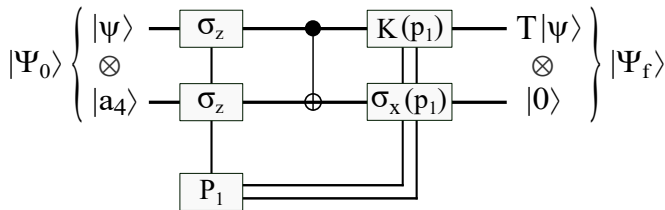


FIG. 9: $\pi/8$ phase gate with $|a_4\rangle \equiv (|\bar{0}\rangle + e^{i\frac{\pi}{4}}|\bar{1}\rangle)/\sqrt{2}$, $K(p_1) \equiv e^{-i\frac{\pi}{8}\sigma_z(1-p_1)}$ and $\sigma_x(p_1) \equiv e^{i\frac{\pi}{4}\sigma_x(1-p_1)}$. $p_1 = \pm 1$ represent measurement results of $P_1 = \sigma_z \otimes \sigma_z$, which are transported via classical channels to the subsequent gates⁸¹.

By fine tuning τ we can achieve $r = e^{i\pi/4}$, which corresponds to $\rho = |a_4\rangle\langle a_4|$. Since fine tuning is topologically not protected, we are just able to create "noisy" copies of $|a_4\rangle$ with a certain error probability $\epsilon^{2,80}$. Nevertheless, for $\langle a_4|\rho|a_4\rangle = 1 - \epsilon \gtrsim 0.86$, these copies can be purified using a $[[15,1,3]]$ Reed-Muller code, which is a special error correction code only including operations from $\mathcal{O}_{\text{ideal}}$ and projective parity measurements. Therefore this code is perfectly realizable with our tTt building block structure⁷⁸. For $\epsilon \ll 1$, the final error probability after one round of purification is given by $\epsilon_{\text{out}} \approx 35\epsilon^3 + \mathcal{O}(\epsilon^4)$ ⁷⁸.

As mentioned above, the ancillary $|a_4\rangle$ state enables the construction of a $\pi/8$ phase gate⁸⁰, which is visualized in Fig. 9. For an arbitrary single qubit state

$$|\psi\rangle \equiv a|\bar{0}\rangle + b|\bar{1}\rangle \quad \text{with} \quad a, b \in \mathbb{C} \wedge |a|^2 + |b|^2 = 1,$$

we define the composite two qubit state

$$|\Psi_0\rangle \equiv |\psi\rangle \otimes |a_4\rangle$$

and measure its eigenvalues with respect to $P_1 \equiv \sigma_z \otimes \sigma_z$. Both eigenvalues $p_1 = \pm 1$ have probability 1/2 and the projected states are given by

$$\begin{aligned} |\Psi_1^+\rangle &= a|\bar{0}, \bar{0}\rangle + be^{i\frac{\pi}{4}}|\bar{1}, \bar{1}\rangle \\ |\Psi_1^-\rangle &= ae^{i\frac{\pi}{4}}|\bar{0}, \bar{1}\rangle + b|\bar{1}, \bar{0}\rangle. \end{aligned}$$

If one subsequently applies a CNOT gate, defining the first qubit as the control qubit, one gets

$$\begin{aligned} |\Psi_2^+\rangle &= (a|\bar{0}\rangle + be^{i\frac{\pi}{4}}|\bar{1}\rangle) \otimes |\bar{0}\rangle \\ |\Psi_2^-\rangle &= (ae^{i\frac{\pi}{4}}|\bar{0}\rangle + b|\bar{1}\rangle) \otimes |\bar{1}\rangle. \end{aligned}$$

Afterwards, if we measured $p_1 = -1$, we apply a K gate to the first and a σ_x gate to the second qubit of $|\Psi_2^-\rangle$, eventually leading to (for both results $p_1 = \pm 1$)

$$|\Psi_{\text{final}}\rangle = (a|\bar{0}\rangle + be^{i\frac{\pi}{4}}|\bar{1}\rangle) \otimes |\bar{0}\rangle.$$

Hence, we realized a $\pi/8$ gate acting on $|\psi\rangle$ ⁸⁰. Similar to the CNOT gate construction in Fig. 7, the above algorithm can be designed with tTt building blocks. In particular, one has to prepare $|a_4\rangle$ in an auxiliary tTt structure next to a tTt block, defining $|\psi\rangle$. To enable the intermediate CNOT operation, one needs to implement another auxiliary tTt building block between these two structures.

So far we did not clarify how to realize projective measurements as well as qubit readout schemes in our nanowire structure. Particularly, one can achieve this by coupling all tTt building blocks to superconducting flux qubits with three Josephson junctions (JJs)^{88,89}. Their qubits are formed by clockwise and counterclockwise supercurrents, separated by an energy gap. Placing charge carriers next to the superconducting islands between the outer JJs closes this gap and therefore enables us to read off the implemented fermion parity

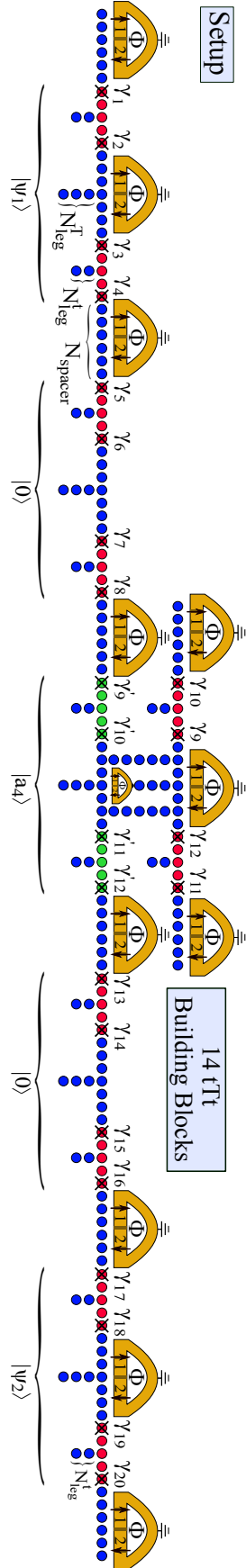


FIG. 10: Hardware setup of a two qubit system, allowing for universal TQC algorithms. The two outer tTt building blocks define the logical qubits $|\psi_{1,2}\rangle$ via their MF modes $\gamma_{1,2,3,4}$ and $\gamma_{17,18,19,20}$. To enable a $\pi/8$ gate for each logical qubit, one has to generate $|a_4\rangle$ in the middle tTt structure. This state is distilled in the top fifteen tTt building blocks via a $[[15,1,3]]$ Reed-Muller code and finally transferred to the ancillary qubit structure, defined by $\gamma'_{9,10,11,12}$. CNOT operations between $|\psi_1\rangle$ and $|\psi_2\rangle$ or between $|\psi_{1,2}\rangle$ and $|a_4\rangle$, can be realized via the two ancillary tTt blocks, hosting the eight MF modes $\gamma_{5,6,7,8}$ and $\gamma_{13,14,15,16}$. They are initialized as stabilizer states $|0\rangle$. Blue sites indicate topologically trivial parameter regions, whereas red ones encode a topologically non-trivial ones. Green sites initially define topologically trivial junction parts, as well. To enable nondestructive, projective measurements, the device is connected to several superconducting flux qubits with islands 1 and 2, which are shown in yellow. More explanations are given in the text.

electromagnetically. This allows the nondestructive, joined parity measurement of MF operator combinations, by bringing them close to these islands^{88,89}.

In Fig. 10, we finally suggest our Majorana based two qubit system, allowing for universal TQC algorithms. Here, the logical qubits $|\psi_{1,2}\rangle$ are defined by $\gamma_{1,2,3,4}$ and $\gamma_{17,18,19,20}$. While all single qubit operations from $\mathcal{O}_{\text{ideal}}$, such as the Hadamard gate H or the phase gate K, can be realized by the braiding of MF modes within the qubits they define, the inner tTt building blocks serve as ancillary qubits for $\pi/8$ and CNOT gate operations. In particular, the ancillary qubits, formed by $\gamma_{5,6,7,8}$ and $\gamma_{13,14,15,16}$, are initialized in stabilizer states $|0\rangle$ and enable the CNOT gate operations by using the protocol given in Eq.(13). In the middle tTt building block, one can implement a purified $|a_4\rangle$ state, allowing for $\pi/8$ gate operations. This state is distilled within the top fifteen tTt building blocks, using the error correction protocol, explained above. After one elementary purification round $\gamma_{9,10,11,12}$ define $|a_4\rangle$ and are subsequently shifted to their final positions, indicated by $\gamma'_{9,10,11,12}$. Additionally, we use superconducting flux qubits with islands 1&2 for the realization of nondestructive projective parity measurements. We want to remark that such measurements can also be performed with superconducting charge qubits in a transmission line resonator⁹⁰. They promise a reduced sensitivity to charge noise, but are much larger in area ($300\mu\text{m}$ vs. $3\mu\text{m}$)^{90,91}. Last but not least, we emphasize that it is possible to horizontally stick together $m \in \mathbb{N}$ of these building blocks. This naturally defines a $2m$ -qubit system.

VII. CONCLUSION & OUTLOOK

In this work, we suggested a Majorana based multi qubit setup, which satisfies all DiVincenzo criteria⁷⁷. This structure is suitable for universal quantum computing, based on Majorana braiding operations, non-Clifford gate distillation protocols, as well as nondestructive, projective measurements. We explicitly simulated the exchange of four Majorana modes on a branched nanowire device, consisting of an inner T-shaped and two outer t-shaped structures. To ensure our computational basis, one has to make sure that the central T-structure is much larger than the two side ones. Moreover, we showed that in the adiabatic limit the Majorana gating time needs to be smaller than the inverse of the squared superconducting gap and scales linearly with the gating potential. Further, we presented a formalism to correct the appearance of additional Majorana modes in very narrow, branched nanowire systems. We explicitly derived an associated correction potential, by using a Green's function approach.

From a broader perspective, there are many non-topological approaches to construct a quantum computer. The explicit decoherence and operation time

Quantum System	T_{de} [s]	T_{op} [s]	n_{op}
Nuclear Spin	10^{-2} - 10^{-8}	10^{-3} - 10^{-6}	10^5 - 10^{14}
Electron Spin	10^{-3}	10^{-7}	10^4
Ion trap (In^+)	10^{-1}	10^{-14}	10^{13}
Single e^- -Au	10^{-8}	10^{-14}	10^6
Single e^- -GaAs	10^{-10}	10^{-13}	10^3
Quantum Dot	10^{-6}	10^{-9}	10^3
Optical cavity	10^{-5}	10^{-14}	10^9
Microwave cavity	10^0	10^{-4}	10^4
Majorana TQC	10^{-4} - 10^{-5}	10^{-8}	10^3 - 10^4

TABLE II: Decoherence T_{de} and operation T_{op} time scales of various quantum computing concepts, as well as the amount of possible quantum bit operations $n_{\text{op}} \equiv T_{\text{de}}/T_{\text{op}}$ ⁷⁷.

scales T_{de} and T_{op} , as well as the amount n_{op} of possible quantum bit operations during T_{de} , are visualized within Tab. II for various qubit systems. We also embedded our TQC approach within this table. Recently, it was shown that the protection of Majorana based qubits against decoherence is heavily influenced by single electron tunneling from external sources, known as quasi-particle poisoning^{92–94}. In our system, the external source is given by the underlying superconductor.

Such processes change the fermion parity, generate bit flips and therefore make successful TQC algorithms impossible. Even worse, MF modes can hybridize with the mentioned states, decay and lose their anyonic features. Thus, the quasi-particle tunneling time scale sets an upper boundary for the coherence time in our device². Recent experiments predict Majorana coherence time scales which are longer than 10ms in proximitized semiconducting nanowires⁹⁵. Hence, if one compares the timescales in Tab. II, takes into account that our quantum algorithms are topologically protected and that all DiVincenzo criteria are satisfied, the present TQC approach is highly interesting for upcoming experimental realizations.

ACKNOWLEDGMENTS

Acknowledgments. We thank Ronny Thomale and Peter Schmitteckert for useful discussions. We acknowledge financial support through the Deutsche Forschungsgemeinschaft (DFG, German Research Foundation) â€ Project-ID 258499086 â€ SFB 1170, the ENB Graduate School on Topological Insulators and through the Würzburg-Dresden Cluster of Excellence on Complexity and Topology in Quantum Matter - ct.qmat (EXC 2147, project-id 39085490). Additionally, this work was financially supported by the German research foundation DFG (Grant No. HA 5893/3-1).

-
- ¹ A. Y. Kitaev, Annals of Physics **303**, 2 (2003).
 - ² S. Das Sarma, M. Freedman, and C. Nayak, NPJ Quantum Information **1**, 15001 (2015).
 - ³ L. Fu and C. L. Kane, Phys. Rev. Lett. **100**, 096407 (2008).
 - ⁴ L. Fu and C. L. Kane, Phys. Rev. B **79**, 161408 (2009).
 - ⁵ A. Cook and M. Franz, Phys. Rev. B **84**, 201105 (2011).
 - ⁶ T.-P. Choy, J. M. Edge, A. R. Akhmerov, and C. W. J. Beenakker, Phys. Rev. B **84**, 195442 (2011).
 - ⁷ A. Kitaev, Annals of Physics **321**, 2 (2006).
 - ⁸ M. Greiter and R. Thomale, Phys. Rev. Lett. **102**, 207203 (2009).
 - ⁹ G. Moore and N. Read, Nuclear Physics B **360**, 362 (1991).
 - ¹⁰ N. Read and D. Green, Phys. Rev. B **61**, 10267 (2000).
 - ¹¹ A. Y. Kitaev, Physics-Uspekhi **44**, 131 (2001).
 - ¹² D. A. Ivanov, Phys. Rev. Lett. **86**, 268 (2001).
 - ¹³ J. D. Sau, R. M. Lutchyn, S. Tewari, and S. Das Sarma, Phys. Rev. Lett. **104**, 040502 (2010).
 - ¹⁴ J. Alicea, Phys. Rev. B **81**, 125318 (2010).
 - ¹⁵ R. M. Lutchyn, J. D. Sau, and S. Das Sarma, Phys. Rev. Lett. **105**, 077001 (2010).
 - ¹⁶ Y. Oreg, G. Refael, and F. von Oppen, Phys. Rev. Lett. **105**, 177002 (2010).
 - ¹⁷ S. R. Elliott and M. Franz, Rev. Mod. Phys. **87**, 137 (2015).
 - ¹⁸ D. Aasen, M. Hell, R. V. Mishmash, A. Higginbotham, J. Danon, M. Leijnse, T. S. Jespersen, J. A. Folk, C. M. Marcus, K. Flensberg, and J. Alicea, Phys. Rev. X **6**, 031016 (2016).
 - ¹⁹ Q. L. He, L. Pan, A. L. Stern, E. C. Burks, X. Che, G. Yin, J. Wang, B. Lian, Q. Zhou, E. S. Choi, K. Murata, X. Kou, Z. Chen, T. Nie, Q. Shao, Y. Fan, S.-C. Zhang, K. Liu, J. Xia, and K. L. Wang, Science **357**, 294 (2017).
 - ²⁰ V. Mourik, K. Zuo, S. M. Frolov, S. R. Plissard, E. P. A. M. Bakkers, and L. P. Kouwenhoven, Science **336**, 1003 (2012).
 - ²¹ L. P. Rokhinson, X. Liu, and J. K. Furdyna, Nature Physics **8**, 795 (2012).
 - ²² M. T. Deng, C. L. Yu, G. Y. Huang, M. Larsson, P. Caroff, and H. Q. Xu, Nano Letters **12**, 6414 (2012).
 - ²³ A. Das, Y. Ronen, Y. Most, Y. Oreg, M. Heiblum, and H. Shtrikman, Nature Physics **8**, 887 (2012).
 - ²⁴ H. O. H. Churchill, V. Fatemi, K. Grove-Rasmussen, M. T. Deng, P. Caroff, H. Q. Xu, and C. M. Marcus, Phys. Rev. B **87**, 241401 (2013).
 - ²⁵ S. Nadj-Perge, I. K. Drozdov, J. Li, H. Chen, S. Jeon, J. Seo, A. H. MacDonald, B. A. Bernevig, and A. Yazdani, Science **346**, 602 (2014).
 - ²⁶ S. M. Albrecht, A. P. Higginbotham, M. Madsen, F. Kuemmeth, T. S. Jespersen, J. Nygard, P. Krogstrup, and C. M. Marcus, Nature Physics **531**, 206 (2016).
 - ²⁷ R. Pawlak, M. Kisiel, J. Klinovaja, T. Meier, S. Kawai, T. Glatzel, D. Loss, and E. Meyer, NPJ Quantum Information **2**, 16035 (2016).
 - ²⁸ M. T. Deng, S. Vaitiekenas, E. B. Hansen, J. Danon, M. Leijnse, K. Flensberg, J. Nygård, P. Krogstrup, and C. M. Marcus, Science **354**, 1557 (2016).
 - ²⁹ Å.-n. Gül, H. Zhang, J. D. S. Bommer, M. W. A. de Moor, D. Car, S. R. Plissard, E. P. A. M. Bakkers, A. Geresdi, K. Watanabe, T. Taniguchi, and L. P. Kouwenhoven, Nature Nanotechnology **13**, 192 (2018).
 - ³⁰ B. E. Feldman, M. T. Randeria, J. Li, S. Jeon, Y. Xie, Z. Wang, I. K. Drozdov, B. Andrei Bernevig, and A. Yazdani, Nature Physics **13**, 286 (2017).
 - ³¹ H. J. Suominen, M. Kjaergaard, A. R. Hamilton, J. Shabani, C. J. Palmstrøm, C. M. Marcus, and F. Nichele, Phys. Rev. Lett. **119**, 176805 (2017).
 - ³² M. Hell, K. Flensberg, and M. Leijnse, Phys. Rev. B **96**, 035444

- (2017).
- 33 H. Zhang, Ö. Gül, S. Conesa-Boj, M. P. Nowak, M. Wimmer, K. Zuo, V. Mourik, F. K. de Vries, J. van Veen, M. W. A. de Moor, J. D. S. Bommer, D. J. van Woerkom, D. Car, S. R. Plissard, E. P. A. M. Bakkers, M. Quintero-Pérez, M. C. Cassidy, S. Koelling, S. Goswami, K. Watanabe, T. Taniguchi, and L. P. Kouwenhoven, *Nature Communications* **8**, 16025 (2017).
 - 34 F. Nichele, A. C. C. Drachmann, A. M. Whiticar, E. C. T. O'Farrell, H. J. Suominen, A. Fornieri, T. Wang, G. C. Gardner, C. Thomas, A. T. Hatke, P. Krogstrup, M. J. Manfra, K. Flensberg, and C. M. Marcus, *Phys. Rev. Lett.* **119**, 136803 (2017).
 - 35 H. Zhang, C.-X. Liu, S. Gazibegovic, D. Xu, J. A. Logan, G. Wang, N. van Loo, J. D. S. Bommer, M. W. A. de Moor, D. Car, R. L. M. Op Het Veld, P. J. van Veldhoven, S. Koelling, M. A. Verheijen, M. Pendharkar, D. J. Pennachio, B. Shojaei, J. S. Lee, C. J. Palmström, E. P. A. M. Bakkers, S. D. Sarma, and L. P. Kouwenhoven, *Nature (London)* **556**, 74 (2018).
 - 36 A. Grivnin, E. Bor, M. Heiblum, Y. Oreg, and H. Shtrikman, *arXiv: 1807.06632* (2018).
 - 37 S. Vaitiekėnas, M.-T. Deng, J. Nygård, P. Krogstrup, and C. M. Marcus, *Phys. Rev. Lett.* **121**, 037703 (2018).
 - 38 C. K. Chiu, M. M. Vazifeh, and M. Franz, *Europhysics Letters* **110**, 10001 (2015).
 - 39 S. Vijay and L. Fu, *Phys. Rev. B* **94**, 235446 (2016).
 - 40 S. Plugge, L. A. Landau, E. Sela, A. Altland, K. Flensberg, and R. Egger, *Phys. Rev. B* **94**, 174514 (2016).
 - 41 L. A. Landau, S. Plugge, E. Sela, A. Altland, S. M. Albrecht, and R. Egger, *Phys. Rev. Lett.* **116**, 050501 (2016).
 - 42 J. Wiedenmann, E. Bocquillon, R. S. Deacon, S. Hartinger, O. Herrmann, T. M. Klapwijk, L. Maier, C. Ames, C. Brüne, C. Gould, A. Oiwa, K. Ishibashi, S. Tarucha, H. Buhmann, and L. W. Molenkamp, *Nature Communications* **7**, 10303 (2016).
 - 43 S. Plugge, A. Rasmussen, R. Egger, and K. Flensberg, *New Journal of Physics* **19**, 012001 (2017).
 - 44 T. Karzig, C. Knapp, R. M. Lutchyn, P. Bonderson, M. B. Hastings, C. Nayak, J. Alicea, K. Flensberg, S. Plugge, Y. Oreg, C. M. Marcus, and M. H. Freedman, *Phys. Rev. B* **95**, 235305 (2017).
 - 45 D. Litinski and F. von Oppen, *Phys. Rev. B* **96**, 205413 (2017).
 - 46 D. Litinski, M. S. Kesselring, J. Eisert, and F. von Oppen, *Phys. Rev. X* **7**, 031048 (2017).
 - 47 F. Domínguez, O. Kashuba, E. Bocquillon, J. Wiedenmann, R. S. Deacon, T. M. Klapwijk, G. Platero, L. W. Molenkamp, B. Trauzettel, and E. M. Hankiewicz, *Phys. Rev. B* **95**, 195430 (2017).
 - 48 E. Bocquillon, R. S. Deacon, J. Wiedenmann, P. Leubner, T. M. Klapwijk, C. Brüne, K. Ishibashi, H. Buhmann, and L. W. Molenkamp, *Nature Nanotechnology* **12**, 137 (2017).
 - 49 C. W. J. Beenakker, *Annu. Rev. Con. Mat. Phys.* **4**, 113 (2013).
 - 50 J. Alicea, *Reports on Progress in Physics* **75**, 076501 (2012).
 - 51 M. Leijnse and K. Flensberg, *Semiconductor Science and Technology* **27**, 124003 (2012).
 - 52 T. D. Stanescu and S. Tewari, *J. Phys.: Condens. Matter* **25**, 233201 (2013).
 - 53 F. L. Pedrocchi and D. P. DiVincenzo, *Phys. Rev. Lett.* **115**, 120402 (2015).
 - 54 F. L. Pedrocchi, N. E. Bonesteel, and D. P. DiVincenzo, *Phys. Rev. B* **92**, 115441 (2015).
 - 55 T. D. Stanescu and S. Das Sarma, *Phys. Rev. B* **97**, 045410 (2018).
 - 56 Y. Huang, J. D. Sau, T. D. Stanescu, and S. Das Sarma, *Phys. Rev. B* **98**, 224512 (2018).
 - 57 M. S. Scheurer and A. Shnirman, *Phys. Rev. B* **88**, 064515 (2013).
 - 58 L.-H. Wu, Q.-F. Liang, and X. Hu, *Science and Technology of Advanced Materials* **15**, 064402 (2014).
 - 59 Q.-B. Cheng, J. He, and S.-P. Kou, *Physics Letters A* **380**, 779 (2016).
 - 60 T. Karzig, F. Pientka, G. Refael, and F. von Oppen, *Phys. Rev. B* **91**, 201102 (2015).
 - 61 C. Sozinho Amorim, K. Ebihara, A. Yamakage, Y. Tanaka, and M. Sato, *Phys. Rev. B* **91**, 174305 (2015).
 - 62 C. Knapp, M. Zaletel, D. E. Liu, M. Cheng, P. Bonderson, and C. Nayak, *Phys. Rev. X* **6**, 041003 (2016).
 - 63 M. Hell, J. Danon, K. Flensberg, and M. Leijnse, *Phys. Rev. B* **94**, 035424 (2016).
 - 64 A. Rahmani, B. Seradjeh, and M. Franz, *Phys. Rev. B* **96**, 075158 (2017).
 - 65 M. Sekania, S. Plugge, M. Greiter, R. Thomale, and P. Schmitteckert, *Phys. Rev. B* **96**, 094307 (2017).
 - 66 B. Bauer, T. Karzig, R. Mishmash, A. Antipov, and J. Alicea, *SciPost Physics* **5**, 004 (2018).
 - 67 J. Alicea, Y. Oreg, G. Refael, F. von Oppen, and M. P. A. Fisher, *Nature Physics* **7**, 412 (2011).
 - 68 C. Sozinho Amorim, K. Ebihara, A. Yamakage, Y. Tanaka, and M. Sato, *Phys. Rev. B* **91**, 174305 (2015).
 - 69 A. C. Potter and P. A. Lee, *Phys. Rev. Lett.* **105**, 227003 (2010).
 - 70 R. M. Lutchyn, T. D. Stanescu, and S. Das Sarma, *Phys. Rev. Lett.* **106**, 127001 (2011).
 - 71 F. Sols, M. Macucci, U. Ravaioli, and K. Hess, *Journal of Applied Physics* **66**, 3892 (1989).
 - 72 Y. K. Lin, Y. N. Chen, and D. S. Chu, *Journal of Applied Physics* **91**, 3054 (2002).
 - 73 R. L. Schult, D. G. Ravenhall, and H. W. Wyld, *Phys. Rev. B* **39**, 5476 (1989).
 - 74 If this assumption is not satisfied this does not mean that we are not able to simulate topological braiding processes. However, for this scenario the extraction of topological phases becomes much more challenging, since the HMF modes are formed by a complex (arbitrary) composition of MF modes $\gamma_{1,2,3,4}$. Moreover, one needs to determine all hybridization amplitudes and derive the associated exchange statistics of HMF modes for each initial parameter configuration. Therefore, such a scenario is rather undesirable.
 - 75 R. R. Puri, *Non-Relativistic Quantum Mechanics* (Cambridge University Press, 2017).
 - 76 D. J. Griffiths, *Introduction to Quantum Mechanics* (Cambridge University Press, 2016).
 - 77 M. A. Nielsen and I. L. Chuang, *Quantum Computation and Quantum Information* (Cambridge University Press, 2011).
 - 78 S. Bravyi and A. Y. Kitaev, *Phys. Rev. A* **71**, 022316 (2005).
 - 79 D. Gottesman, *arXiv:9807006* (1998).
 - 80 S. Bravyi, *Phys. Rev. A* **73**, 042313 (2006).
 - 81 T. Hyart, B. van Heck, I. C. Fulga, M. Burrello, A. R. Akhmerov, and C. W. J. Beenakker, *Phys. Rev. B* **88**, 035121 (2013).
 - 82 T. Karzig, Y. Oreg, G. Refael, and M. H. Freedman, *Phys. Rev. X* **6**, 031019 (2016).
 - 83 L. S. Georgiev, *Phys. Rev. B* **74**, 235112 (2006).
 - 84 M. B. Hastings, *arXiv:1703.00612* (2017).
 - 85 A. de Vries, *Quantum Computation. An Introduction for Engineers and Computer Scientists* (Books On Demand, 2012).
 - 86 S. Bravyi and A. Y. Kitaev, *Annals of Physics* **298**, 210 (2002).
 - 87 O. Zilberberg, B. Braunecker, and D. Loss, *Phys. Rev. A* **77**, 012327 (2008).
 - 88 F. Hassler, A. R. Akhmerov, C.-Y. Hou, and C. W. J. Beenakker, *New Journal of Physics* **12**, 125002 (2010).
 - 89 R. P. Tiwari and D. Stroud, *Phys. Rev. B* **76**, 220505 (2007).
 - 90 F. Hassler, A. R. Akhmerov, and C. W. J. Beenakker, *New Journal of Physics* **13**, 095004 (2011).
 - 91 J. Clarke and F. K. Wilhelm, *Nature Physics* **453**, 1031 (2008).
 - 92 J. C. Budich, S. Walter, and B. Trauzettel, *Phys. Rev. B* **85**, 121405(R) (2012).
 - 93 G. Goldstein and C. Chamon, *Phys. Rev. B* **84**, 205109 (2011).
 - 94 D. Rainis and D. Loss, *Phys. Rev. B* **85**, 174533 (2012).
 - 95 A. P. Higginbotham, S. M. Albrecht, G. Kiršanskas, W. Chang, F. Kuemmeth, P. Krogstrup, T. S. Jespersen, J. Nygård, K. Flensberg, and C. M. Marcus, *Nature Physics* **11**, 1017 (2015).